Atmos. Meas. Tech. Discuss., 3, 1263–1301, 2010
www.atmos-meas-tech-discuss.net/3/1263/2010/

Atmospheric Measurement Techniques Discussions

This discussion paper is/has been under review for the journal Atmospheric Measurement Techniques (AMT). Please refer to the corresponding final paper in AMT if available.

Carbon monoxide mixing ratios over Oklahoma between 2002 and 2009 retrieved from Atmospheric Emitted Radiance Interferometer spectra

L. Yurganov[1], W. McMillan[1], C. Wilson[1], M. Fischer[2], and S. Biraud[2]

[1]Joint Center for Earth Systems Technology, University of Maryland, Baltimore County, Baltimore, MD, USA
[2]Lawrence Berkeley National Laboratory, Berkeley, CA, USA

Received: 7 February 2010 – Accepted: 12 March 2010 – Published: 29 March 2010

Correspondence to: L. N. Yurganov (yurganov@umbc.edu)

Published by Copernicus Publications on behalf of the European Geosciences Union.

Abstract

CO mixing ratios weighted over the bottom 2-km thick atmospheric layer between 2002 and 2009 were retrieved from downwelling infrared (IR) radiance spectra of the clear sky measured by a zenith-viewing Atmospheric Emitted Radiance Interferometer (AERI) deployed at the Southern Great Plains (SGP) observatory of the Atmospheric Radiation Measurements (ARM) Program near Lamont, Oklahoma. A version of the algorithm proposed by He at al. (2001) was significantly improved and validated. Essentially, the new algorithm retrieves a CO mixing ratio that is determined by the convolution of the a priori profile (assumed to be constant with altitude), the true profile, and the averaging kernel which maximizes near the surface. Approximately 70% of the CO signal comes from the boundary layer and the remaining 30% come from the lower part of the free troposphere. Archived temperature and water vapor profiles retrieved from the same AERI spectra through automated ARM processing were used as input data for the CO retrievals. We found the archived water vapor profiles required additional constraint using SGP Microwave Radiometer retrievals of total precipitable water vapor. Additionally, a correction for scattered solar light was developed. The retrieved CO was validated using simultaneous independently measured CO profiles. An aircraft supplied in situ CO measurements at altitudes up to 4572 m above sea level once or twice a week between March 2006 and December 2008. The aircraft measurements were supplemented with ground-based CO measurements at the SGP and retrievals from the Atmospheric IR Sounder (AIRS) above 5 km to create full tropospheric CO profiles. Comparison of the convolved profiles to the AERI CO retrievals found a squared correlation coefficient of 0.57, a standard deviation of ±11.7 ppbv, a bias of 16 ppbv, and a slope of 0.92. Averaged seasonal and diurnal cycles measured by AERI are compared with those measured continuously in situ at the SGP in the boundary layer. Monthly mean CO values measured by AERI between 2002 and 2009 are compared with those measured by AIRS over North America, the Northern Hemisphere mid-latitudes, and over the tropics.

AMTD

3, 1263–1301, 2010

1 Introduction

Carbon monoxide is a by-product of any combustion, both anthropogenic and natural (e.g., wild fires), and a result of photochemical conversion from methane and other carbonaceous gases (Bergamaschi et al., 2000). Primarily, it is removed from the atmosphere through reaction with hydroxyl (OH) (Spivakovsky et al., 2000). CO is a relatively short-lived gas (life time ~2 months) conveniently measured in situ using gas-chromatography, non-dispersive IR technique, diode lasers, open path FTIR (Novelli et al., 2003; Jaffe et al., 1998; Nedelec et al., 2003; Sachse et al., 1987; Goode et al., 1999). Sun-viewing spectrometers supply remotely sensed CO total column amounts and rough vertical distribution (e.g., Dianov-Klokov and Yurganov, 1981; Zander et al., 1989; Rinsland et al., 1998). Space-based remote sensing IR spectroscopic techniques (Reichle et al., 1990; Edwards et al., 2006; McMillan et al., 2005; Buchwitz et al., 2004; Turquety et al., 2009) provide information about CO mixing ratio in the free troposphere. CO is widely used as a tracer of biomass burning (McMillan et al., 2008a, b; Edwards et al., 2004; Turquety et al., 2009) and anthropogenic pollution (McMillan et al., 2008a, 2010; Clerbaux et al., 2008). CO measurements are helpful for validation of Chemistry Transport Models (CTM) (Zhang et al., 2008), and as input information for source inversion models (Kopacz et al., 2010; Fisher et al., 2010).

This paper presents results of remote sensing CO measurements using the Atmospheric Emitted Radiance Interferometer (AERI) at the Southern Great Plains (SGP) site of the United States Department of Energy (DOE) Atmospheric Radiation Measurement (ARM) Program. The ARM program was created in 1989 with the primary objective of improving scientific understanding of the fundamental physics related to interactions between clouds and atmospheric radiation (ACRF Annual Report, 2008). ARM focuses on obtaining continuous field measurements and providing data products that promote the advancement of climate models. The program has become a diverse endeavor contibuting to many fields of atmospheric physics and chemistry. One of these important new fields is the carbon cycle.

AMTD
3, 1263–1301, 2010

Wang et al. (1999) and He et al. (2001) reported the first results of CO retrievals from AERI SGP spectra for a short period between 2 and 4 March 1998 using a code specified here as version 1 (v1). In the present paper, the v1 retrieval algorithm was improved and is designated now as version 2 (v2). Here, we present validation and analysis of CO retrievals from the SGP AERI from 2002 through 2009. The laborious improvements to the AERI v1 CO retrieval algorithm are documented. A more comprehensive analysis of this data set, possibly extended back to 1997, will be the subject of future publications.

The SGP AERI CO retrievals between February 2006 and December 2008 are validated using 3 independent, simultaneous, and collocated sets of CO data: (i) quasi-continuous in situ measurements of CO mixing ratios from a 60 m tower (Biraud et al., 2007), (ii) in situ CO profiles measured by aircraft between 83 m and 4000 m above the ground (Sweeney, 2010), and (iii) CO profiles retrieved from a space-borne AIRS sounder for altitudes above 5 km (McMillan et al., 2009). The 7.5-year period of AERI CO retrievals, 1 January 2002 through September 2009, is analyzed and interpreted in terms of changes in fossil fuel and biomass burning emissions.

2 Location, instrument, and retrieval procedure

The SGP site (36°36′18.0″ N, 97°29′6.0″ W) is located in northern Oklahoma southeast of the town of Lamont. The heart of the SGP site is the heavily instrumented central facility surrounded by cattle pasture and wheat fields. The instruments throughout the site autonomously collect data on surface and atmospheric properties and routinely pass this data to the Site Data System which is linked by high-speed communications to the ARM Archive and Data Center. The collected data and derived products are archived and publicle available online (http://www.archive.arm.gov).

The AERI measures the downwelling absolute infrared spectral radiance (in watts per square meter per steradian per wavenumber) emitted by the sky directly above the instrument (Knuteson et al., 2004; Garcia et al., 2004). The AERI spectra can be

AMTD
3, 1263–1301, 2010

used for investigation of boundary layer (BL) temperature and water vapor distributions (Feltz et al., 1998; Smith et al., 1999; Turner et al., 2000), cloud properties (Collard et al., 1995; DeSlover et al., 1999; Turner et al., 2003), carbon monoxide retrievals (He et al., 2001), and other applications (Minnett et al., 2001; Nalli et al., 2008). AERI measurements cover the spectral range from 520 to 3300 cm^{-1} (3–19.2 µm) with an unapodized spectral resolution of 1.0 cm^{-1} (1 cm optical path delay). The instrument field-of-view is 1.3 degrees. In normal operation, a calibrated sky radiance spectrum (3 min average) is produced approximately every 8 min utilizing views of two precisely monitored high emissivity calibration black-bodies (Knuteson et al., 2004; Garcia et al., 2004.).

An example spectrum of atmospheric zenith sky radiances measured by the SGP AERI on 30 July 2006 is plotted in Fig. 1. One line of the P-branch and nine lines of the R-branch of the CO 1-0 fundamental vibration-rotation band appear as spikes in the radiance spectrum at the frequencies indicated by the green circles. Other spikes in the inset spectrum arise from water vapor emission. Two transparent intervals (windows) represent spectral intervals with minimal contribution from atmospheric gases. However, radiation emitted and scattered by aerosols, thin clouds, and other sources influence measurements in the spectral windows. For example, during the day time, a tail of the solar radiation scattered by aerosols and thin clouds often shows up between 2500 and 3000 cm^{-1}. The contribution of this solar radiance for the interval between 2130 and 2190 cm^{-1} should be small, but it is variable both diurnally and day-to-day due to aerosol scattering. This scattered sunlight depends on the solar zenith angle, aerosol abundance, and the presence of thin clouds (especially cirrus). Spectra with thick clouds are removed from our analysis as discussed below.

The basic AERI CO retrieval procedure was originally developed and validated for retrievals from space- and air-borne IR spectra (McMillan et al., 1996, 1997, 2003) and subsequently modified for retrievals from AERI spectra (Wang et al., 1999; He et al., 2001). Due to the lower spectral resolution of AERI compared to the Network for the Detection of Atmospheric Composition Change (NDACC) solar transmission

instruments, a straightforward Non-Linear-Least-Squares iterative approach such as the SFIT2 algorithm developed for narrow microwindows (Rinsland et al., 2005) is not appropriate. Until we develop a fast spectral computation routine (forward model), we use the one-parameter (CO abundance) retrieval algorithm first published in McMillan et al. (1996) and described in more detail in McMillan et al. (1997).

Radiative transfer calculations are performed using the k-Compressed Atmospheric Radiative Transfer Algorithm (kCARTA) (De Souza-Machado et al., 1997). Temperature and water vapor profile retrievals are performed by automated ARM processing using standard AERI software developed by the University of Wisconsin (Feltz et al., 1998) and downloaded from the online ARM archive. These temperature and water vapour profiles are retrieved from other portions of the same AERI spectra using the Rapid Update Cycle-2 (RUC2) or Global Forecast System (GFS) model upper atmosphere (Feltz et al., 1998; Smith et al., 1999; Turner et al., 1999; Feltz et al., 2003). In the v1 and v2 CO retrieval algorithms, a constant tropospheric CO mixing ratio profile (from 100 mb to the surface) is perturbed from the initial value of 100 ppb to minimize the spectral residuals due to CO. However, the vertical sensitivity of this technique is not flat. Figure 2 shows a representative averaging kernel for the v2 CO retrieval algorithm and indicates that approximately 70% of the signal comes from the boundary layer, with the rest of the troposphere contributing the remaining 30% (McMillan et al., 1999). The AERI CO averaging kernels and this figure are discussed in more detail in Sect. 3.

As detailed in McMillan et al. (1997), a brightness temperature spectrum is calculated for constant tropospheric CO mixing ratios using the best available spectral constants from the HITRAN-2004 compilation (Rothman et al., 2005) and the aforementioned AERI temperature/H_2O retrieved profiles. Then a difference (or residual) between a calculated and the measured spectrum is derived. As a result of the regular spacing of the CO lines, the shape of this residual at AERI's 1 cm^{-1} resolution is nearly sinusoidal. The amplitude of this CO signal is proportional to the difference in column CO between the observed and calculated spectrum. Only one piece of information about CO (namely, vertically weighted mixing ratio) is retrieved from each spectrum. Utiliz-

AMTD
3, 1263–1301, 2010

ing a standard Fourier signal processing technique (not to be confused with a Fourier Transform Spectrometric technique), called the Welch method (Candy, 1988; Fante, 1988), we can quantify the amplitude of the sinusoidal residual with a good rejection of H_2O contamination. Spectral residuals are computed for constant CO mixing ratios of 50, 100, 200, and 400 ppbv and a cubic interpolation is applied to the cross-spectral density computed via the Welch method to retrieve the best fit constant CO mixing ratio (McMillan et al., 1997). In spite of its relative simplicity, this technique ensures a good retrieval accuracy (better than 10%) combined with relatively fast spectra processing (1–2 min per spectrum) (He et al., 2001).

The basic cloud filtering technique is described by He et al. (2001). Spectra contaminated by thick or low clouds exhibit a low brightness contrast within the 2100–2200 cm^{-1} spectral range. Low contrast results in lower retrieved CO. Although this spectral contrast shows some seasonality, He et al. (2001) found contrasts <40 K between the most transparent and opaque portions of the 2100–2200 cm^{-1} spectral range indicate the presence of clouds. However, this filtering alone does not find all clouds. Thin clouds, especially cirrus, may display a contrast >40 K, yet their presence can influence the 2100–2200 cm^{-1} spectral region by scattering of solar photons during the day. The effect of these clouds can be comparable to solar scattering by aerosols. A method of correction for such cases is described below.

Five major sources of error influence the accuracy of the retrieved CO: spectral noise, errors in the retrieved temperature profiles, errors in the retrieved H_2O profiles, emission from aerosols and thin clouds, and scattered sunlight. The spectral noise in the CO region (2100–2200 cm^{-1}) is on the order of 0.005 $mW/(m^2\,sr\,cm^{-1})$. Using simulated spectra computed from a set of real continental profiles over the United States with realistic RMS errors of 1 K in temperature profile and simulated water vapor, McMillan et al. (1999) estimated the impacts on CO retrievals. Spectral noise causes an error of about 0.75% in the retrieved CO. RMS temperature profile errors result in errors of about 1.5% in retrieved CO. RMS errors in the water vapor profile can result in CO retrieval errors of several percent. However, systematically biased water vapor pro-

AMTD
3, 1263–1301, 2010

files, errors in precipitable water vapor (PWV), can lead to more substantial errors in retrieved CO as discussed in the following subsection.

Ongoing research is investigating the possibility of simultaneously retrieving BL and mean free tropospheric (MFT) CO mixing ratios from AERI spectra. Preliminary sensitivity studies indicate this should be possible roughly 75% of the time. In addition, work will soon start on a new fast radiative transfer algorithm to enable reprocessing of AERI spectra for CO, CO_2, and CH_4 retrievals. Parallel research with collaborators at the University of Wisconsin-Madison includes improvements to the AERI temperature and water vapor retrieval algorithms.

2.1 Influence of water vapor profile errors on AERI CO retrievals

To estimate the impact of systematic PWV errors on retrievals of CO from AERI spectra, we employed independent measurements of PWV made by the SGP Microwave radiometer (MWR) (Liljegren, 1994). Turner et al. (2007) investigated the accuracy of the MWR PWV and found the disagreement with coincident scanning Raman lidar (Fig. 3a) and radiosondes was well below ±10%. Although generally well correlated, we have found the differences between AERI and MWR PWV can be as large as 20–40%. The largest discrepancies appear for PWV >3 cm (Fig. 3b) where AERI often overestimates PWV. However, we note that for PWV <3 cm, agreement between AERI and MWR PWV is much better.

Figure 4 presents an example of the impact of PWV on CO retrievals for a humid summer day, 30 July 2006. The top panel shows PWV measured by MWR and AERI. AERI PWV increased instantly, from one AERI spectrum to the next, around 03:00 UTC (21:00 local time) and rapidly decreased around 12:00 UTC (06:00 local time); MWR PWV changes much more gradually. We assume that the MWR measurements are more precise. The bottom panel illustrates the impact of this PWV error on the retrieved CO. Variations in the retrieved CO using the AERI water vapor profiles closely follow the temporal variations in AERI PWV. However, CO retrievals using the AERI profiles scaled by the MWR PWV are much smoother but show temporal trends independent

AMTD
3, 1263–1301, 2010

of the MWR PWV. Our v2 AERI CO retrieval algorithm scales the AERI retrieved water vapor profiles by the uniform ratio of PWV_{MWR}/PWV_{AERI} determined separately for each AERI spectrum.

2.2 Influence of scattered light

The version of kCARTA used in this work calculates radiances for aerosol-free and cloud-free atmospheres and it uses empirically based corrections for water vapor continuum emission/absorption. It does not take into account continuum emission/absorption from any short-lived complexes of molecules, e.g., water dimers. Because clouds and aerosols are not included, there is no accounting for scattered sunlight. To estimate contributions from these ignored factors, observed radiances in two transparent intervals of the spectra, 2142.7–2144.1 cm^{-1} and 2167.2–2168.7 cm^{-1} (black bars in Fig. 1), are compared to those calculated by kCARTA. Figure 5 demonstrates that this radiance difference (RD) mostly lies inside the limits ±0.1 mW/(ster m^2 cm^{-1}) for the entire range of PWV experienced at the SGP. For PWV <3 cm RD is slightly positive on average: (0.04 ± 0.04) in the same units. At larger PWV, RD diminishes and becomes negative for the largest observed PWV. Overall, the RD is slightly larger during day time than at night.

We believe the RD pattern evident in Fig. 5 arises from an incomplete accounting for the following sources of radiation: (i) emission from aerosols and thin clouds themselves, (ii) water vapor continuum emission/absorption, and (iii) sunlight scattered from aerosols and clouds. Cases with thick clouds are removed by the previously discussed cloud filter procedure. Emission from aerosols and thin clouds themselves would be expected to exhibit no diurnal variation and should not depend on the total amount of water vapor, i.e., PWV. Although an error in water vapor continuum also should show no diurnal variation, it would display an increasingly significant impact with both PWV and temperature. Obvioulsy, scattering of solar photons should correlate strongly with the solar zenith angle and be maximal around noon.

AMTD
3, 1263–1301, 2010

The quasiconstant positive RD for PWV <3 cm is consistent with the presence of emission from aerosols and thin clouds in the measured spectra ignored by the forward model. Little diurnal variation is apparent. The lowest RD is close to zero and occurs on the clearest days. For >3 cm, a decreasing trend appears. This negative trend might be explained by an overestimation of water vapor continuum emission which is more evident as the atmospheric water vapor amount and temperature increase.

The solar radiation scattered by aerosols is expected to have a maximum at local solar noon (~18:30 UTC). Three examples of cloud-free days in 2006 are given in Fig. 6 (another example is displayed in Fig. 10). Anticorrelation between single measurements of CO and corresponding radiance errors is obvious (squared correlation coefficients are around −0.7), particularly for 18 and 20 June. Moreover, the time-series of retrieved CO for these two days exhibits a minimum roughly symmetric about local solar noon, ~18:30 UTC. Absent other factors and assuming constant CO, the retrieved CO would minimize at solar noon due to the filling in of the transparent CO line wings by scattered solar photons. However, the amount of solar scattering also depends on the amount (total optical depth), type, and vertical distribution of aerosols present. This variation is evident in the different slopes of regression lines S (bottom panel) for these three days varying between −60 and −164 ppb/mW/(m^2 sr^1 cm^{-1}). This, and even larger, range of regression slopes is representative of the entire SGP AERI CO retrieval data set. Thus, it is impossible to determine a single value of S that fits most of data.

Figure 7 illustrates our second attempt to derive a correction algorithm for scattered sunlight through examination of the mean diurnal cycle of retrieved CO from all 2006 AERI spectra. Obviously the v1 CO retrievals (bottom curve, blue with pink diamonds) are anticorrelated with the mean RD (top curve, thin black line). The other curves represent linear subtraction of S*RD values to the hourly mean v1 CO retrievals. Trial values of S range from 0 (i.e., CO v1) to −190. As the value of S increases, the anticorrelation evolves into a correlation. The case with S = −40 is close to the minimal correlation between CO and RD. We chose this value of S for correction of scattered

AMTD
3, 1263–1301, 2010

sunlight in the v2 AERI CO retrievals. However, on average, a 7 ppb diurnal cycle of CO remains even after correction. This diurnal cycle might be real and will be compared with in-situ measurements in the discussion section.

3 Validation

As previously mentioned, three independent correlative data sets were used to build composite ground-truth CO profiles at the SGP site for validation of AERI CO retrievals: (i) quasi-continuous in situ CO measurements from 60 m tower at the SGP (Biraud et al., 2007) , (ii) in situ CO profiles measured by aircraft between 83 m and 4000 m above the ground above the SGP (Sweeny, C., personal communication, 2010) , and (iii) CO profiles retrieved from AIRS for altitudes above 5 km (McMillan et al., 2009). An example composite profile is plotted in Fig. 2.

In situ CO measurements from the 60 m tower (413 m a.s.l. at the foot) at the SGP site are acquired by the Lawrence Berkeley National Laboratory (LBNL) using a non-dispersive infrared gas correlation instrument (Thermo Scientific TE-48C). This instrument has been modified with additional pressure control, frequent zero correction and multi-point calibrations to provide precision and accuracy near 5 ppbv judged by comparison with NOAA network flask measurements (Potosnak et al., 1999).

The in situ CO profiles at the SGP site are measured weekly by the NOAA Earth System Resources Laboratory (ESRL) using an automated programmable flask package operated on a small aircraft. The flasks are filled by air at standard heights above sea level (a.s.l.): 457.2, 609.6, 914.4, 1219.2, 1524.0, 1828.8, 2438.4, 3048.0, 3657.6, 4572.0 m a.s.l. (the surface altitude at SGP is 374 m a.s.l.). The flasks are returned to NOAA/ESRL for analysis via gas chromatography to determine CO mixing ratios (Novelli et al., 1998). Measurements are reported in units of nanomol/mol (10^{-9} molCO per mol of dry air, or parts per billion, ppbv, or ppb) relative to the WMO CO scale (Novelli et al., 1991, 1993). Reproducibility of the measurements, based on repeated analysis of air from a high-pressure cylinder, is 1 ppb at 50 ppb and 2 ppb at 200 ppb. From

AMTD
3, 1263–1301, 2010

2006–2008 there were 98 days when the time of aircraft sounding ±0.5 h matched both AERI and in situ data.

AIRS CO data, version 5, level 3 for ascending orbits, i.e. around noon local time, were used to characterize the CO distribution above 5 km. As illustrated in Fig. 2, AERI sensitivity to these altitudes is small and the ±10% accuracy of AIRS northern hemispheric CO retrievals (McMillan et al., 2009) is quite sufficient for our goals.

The sensitivity of the CO abundance retrieved from an AERI spectrum to the CO amount at different heights is quantified by the averaging kernel (AK) as is common to all inverse techniques (Backus and Gilbert, 1970; Conrath, 1972; Rodgers and Connor, 2003). Because of the formulation of the AERI CO retrieval algorithm, AKs must be computed by brute force. That is, layer by layer we perturb the CO abundance, compute a new spectrum, and perform a CO retrieval on the perturbed spectrum. The difference between the CO amount retrieved from the unperturbed spectrum and that retrieved from the perturbed spectrum yields the sensitivity to the perturbed layer. The ensemble of these differences yields the AK. Using the standard 100 pressure layers in kCARTA requires performing 101 CO retrievals (unperturbed + 100 perturbations). Thus, AKs were calculated only for each day with a matching validation profile. As illustrated in Fig. 2, the AERI CO AK typically is rather broad with a maximum at or just above the surface.

In practice, AERI CO AKs were calculated using jacobians computed by the kCARTA forward model. This greatly speeds the computation of the perturbed spectra as described below. For each matching day, the mean temperature and water vapor profiles retrieved from AERI spectra near the time of the aircraft profile were input to kCARTA along with a 100 ppbv constant tropospheric CO mixing ratio profile to produce a baseline synthetic downwelling infrared spectrum and jacobians on the standard kCARTA 100 pressure layers. The jacobian for each layer is defined as

$$\frac{\Delta\text{Radiance}}{\Delta\text{Carbon Monoxide}}$$

AMTD
3, 1263–1301, 2010

Therefore, the radiance change due to a perturbation in CO is simply given by multiplying each level's jacobian by the magnitude of the CO change. Because the jacobians are valid only for small changes in gas amount, we chose a 5% perturbation factor for each layer. First, the v1 AERI CO retrieval algorithm is run on the unperturbed atmosphere to compute the baseline CO retrieval. Next, the v1 AERI CO retrieval algorithm is run 100 times using each level's radiance change plus the original downwelling infrared spectrum from kCARTA. A larger value of carbon monoxide retrieved for the perturbation of a given pressure layer indicates the retrieval's increased sensitivity to that layer. The ensemble of retrieved CO differences is defined as the AK by the following equation:

$$\mathrm{AK}_i = \frac{\text{Retrieved CO}_i - \text{Base CO}}{\text{Delta CO}_i},$$

where i = index from 1 to 100 of the standard kCARTA pressure layers, AK_i = averaging kernel value for layer$i$, Retrieved CO_i = the retrieved constant tropospheric CO mixing ratio from the spectrum computed by perturbing the CO amount in layer I, Base CO = the retrieved constant CO mixing ratio from the unperturbed spectrum, Delta CO_i = the change in CO in layer i.

The resulting averaging kernel is a unit-less number for each of the 100 kCARTA radiative transfer layers corresponding to the sensitivity of the AERI v1 CO retrieval algorithm to a change in gas amount in each layer. Perhaps more important than the graphical visualization of AERI's vertical sensitivity, the averaging kernels are crucial to quantitative validation of the retrieval algorithm. Following Rodgers and Connor (2003), the composite ground-truth CO vertical profiles ($\mathrm{True}_{\mathrm{CO}}$) were convolved with the a priori 100 ppbv constant tropospheric mixing ratio profile ($\mathrm{Apriori}_{\mathrm{CO}}$) and the averaging kernel (AK) for each matching day to convert the composite ground-truth profile to the AERI CO retrieval algorithm measurement space (a constant tropospheric profile) using the follow matrix equation:

$$\mathrm{Convolved}_{\mathrm{CO}} = \mathrm{Apriori}_{\mathrm{CO}} + \mathrm{AK} * (\mathrm{True}_{\mathrm{CO}} - \mathrm{Apriori}_{\mathrm{CO}})$$

AMTD
3, 1263–1301, 2010

Figure 8 presents the comparison of $Convolved_{CO}$ to the AERI v2 retrieved CO for the 98 matching days. Overall, the AERI v2 retrievals (with a slope of dependence on RD $S = 40$, as chosen above) are biased low by ∼16 ppbv with a standard deviation (STD) of individual data points of ±11.7 ppbv, and a squared correlation coefficient $R^2 = 0.57$. For comparison, the original AERI v1 CO retrievals are shown and exhibit a larger negative bias. A stronger dependence of CO on RD (not shown) with a slope $S = -160$ improves the bias (−9.2 ppbv), STD (±9.6 ppbv), and R^2 (0.65), and STD = ±9.6 ppbv. However, as discussed with Fig. 7, $S = -160$ distorts the mean diurnal cycle. Thus, we have chosen $S = -40$ for the v2 scattered sunlight correction. Concluding this section, data users are advised to refer to RD as a flag for CO retrieval accuracy; for RD>0.05 an additional negative error in retrieved CO around noon of up to 10–12 ppb is possible.

4 Results and discussion

4.1 Diurnal cycle

Figure 9 illustrates a typical example of CO behavior inside the BL (in situ, 60 m tower) and the weighted average for the bottom 2 km layer of the atmosphere supplied by AERI retrievals. The small scatter for both data sets practically disappears after hourly averaging. On this day, the differences between v1 and v2 of the AERI CO retrieval are small with a maximum near noon of ∼5 ppbv. The diurnal cycles of BL CO and that retrieved from AERI are significantly different. The large increase in tower CO overnight could be due to trapping of surface CO emissions in a thin nocturnal boundary layer. AERI's sensitivity to a greater depth of the atmosphere would mute this impact resulting in the apparent differences. Close to dawn, this stable layer is mixed and the tower values decline as CO is vertically redistributed. This redistribution has little impact on the AERI retrievals due to its significant vertical averaging.

AMTD
3, 1263–1301, 2010

Figure 10 gives an example of a clear summer day with a maximum effect of scattered sunlight on the CO retrievals. The tower measurements indicate no accumulation of CO in the BL during the night. The empirical slope of CO versus RD around noon amounts to −192 and the AERI v2 underestimation may be as large as 12 ppb at noon. For other days not shown here, long-range transport of CO above the boundary layer can appear as increases in AERI retrieved CO while the tower sees only the local in situ conditions. Further analysis of such cases is beyond the scope of this study and will be pursued in future publications.

As shown in Fig. 11, the average 2006 diurnal cycle exhibits very similar features to those presented for the one individual day in Fig. 9, although the STDs for both in situ and AERI CO are rather large. The amplitude of the mean diurnal cycle is ∼15.7 ppbv for the in-situ tower data and ∼7.2 ppbv for AERI v2 CO retrievals. On average, BL CO increases during the night for ∼10 h before relaxing back during the other ∼14 h. Not only is the AERI amplitude smaller, the increase appears to be shorter (increasing for ∼8 h and relaxing longer ∼16 h) and out of phase with the BL CO diurnal cycle. Most likely, some of this phase difference results from the incomplete removal of the scattered sunlight artifact in AERI v2 CO retrievals around noon.

4.2 Seasonal cycles and interannual variations

Throughout 2006, 2007, and 2008, both the tower in-situ and AERI remote sensing instruments operated simultaneously at the SGP site. Figure 12 compares the three seasonal cycles for these years. The general shapes of the CO seasonal cycles for both sensors agree with the usually observed CO cycle first measured by Dianov-Klokov and Yurganov (1981): maximum in spring and minimum in late summer or early autumn. The first two annual cycles are similar with the summertime differences perhaps due to transport from distant forest fires (cf. McMillan et al., 2010). Until July 2008, CO did not differ from what was measured during previous years. However, since August 2008, and especially in November and December, both sensors recorded CO mixing ratios 10–20 ppbv lower than during the two previous years. The influence

AMTD
3, 1263–1301, 2010

of smaller CO emissions from fossil fuel burning is the most likely explanation of this effect. Was this just a local effect or a larger scale feature? Below, we compare the SGP observations to satellite data.

Figure 13 presents the anomaly of CO for 2002–2009. The seasonal cycle averaged over January 2004–December 2007 was subtracted from the monthly mean CO data. Calculation of the anomaly is equivalent to deseasonalizing the data. Then, anomalies of monthly means were divided by the mean 2004–2007 seasonal cycle and plotted in percent. Similar anomalies of CO total column measured by AIRS are given for comparison. AIRS CO total columns were averaged for the NH mid latitudes, for North America, and for the tropics. The most substantial positive anomalies were observed in 2002 and 2003. As Yurganov et al. (2005) found, Siberian fires during that time affected the entire Northern Hemisphere: total column CO increased by 20%, and surface mixing ratios increased by 35% (in comparison with 2000–2001). The 25% increase observed by AERI at SGP lies between those two estimates. The differences between total column and surface measurements reflect the intermediate coverage of the AERI CO retrieval averaging the lowest 2 km of the atmosphere.

The largest negative anomaly was observed by the two sensors around January 2009 (a similar effect was observed by MOPITT, according to Yurganov et al., 2009). Is the decrease of CO over the SGP, North America, and the entire NH a result of CO emission diminution from fossil fuel burning triggered by the economic recession? A more comprehensive study including all available data and global chemical transport modeling is necessary. However, at this point, the coincident timing of the minimum for SGP, North America and the NH in January 2009 could be evidence for this. During November, December, and January wild fire activity inside the NH mid-latitudes is almost lacking and its influence on CO burden is minimal. Furthermore, an examination of the Global Fire Emission Data (GFED2) inventory by Yurganov et al. (2009) found little change in this minimal fire activity in the NH in late 2008 and early 2009. In contrast, Yurganov et al. (2009) reported lower than usual CO burdens measured by MOPITT and AIRS in the tropics as shown in Fig. 13. GFED2 also indicated

AMTD
3, 1263–1301, 2010

a lower than usual amount of fire activity in Brazil and Indonesia in the second half of 2008 (Yurganov et al., 2009).

Concluding this section, the influence of tropical CO emissions on the NH mid-latitudes must be quantified, and the timing of transport from the tropics to the NH mid-latitudes must be determined. The three month temporal lag of CO burden minima between the tropics and NH mid-latitudes could result from transport of lower CO burdens from south to north. The smaller percent decrease in the tropics than in the NH should not be misleading: the tropics contain about half of the global air mass and the absolute values of CO burden anomaly are higher there than in the NH. Most likely, however, the NH CO burden in 2008–2009 decreased due to a combination of changes in the CO emissions inside the NH and smaller transport from the tropics.

5 Conclusions

Spectra of downwelling IR radiance acquired by AERIs at the ARM network, including SGP, contain very useful information about trace gases. Other than water vapor, CO is the most easily retrievable trace gas from these spectra. This paper describes an improved algorithm for CO retrieval. It is based on AERI measurements of the downwelling IR radiance in the CO fundamental band. Temperature and water vapor profiles retrieved from the same spectra are important input parameters for this algorithm, but they must be augmented by additional measurements of the total amount of water in the atmosphere. Retrievals of PWV from the MWR instrument at SGP were used to scale the less accurate AERI water vapor retrievals. In addition, the version of kCARTA employed as a forward model neglects scattering of sunlight by aerosols and clouds. This study proposes an empirical correction to account for the additional scattered radiation using measured radiances in the most transparent portions of the CO band. The radiance difference (RD) between this measured radiance and that calculated by the forward model usually is small. In some cases, however, incoming solar radiance scattered by aerosols or clouds is significant, and RD is higher than usual. Unfortunately,

AMTD
3, 1263–1301, 2010

we failed to determine uniform dependence between CO errors and RD. The AERI v2 CO algorithm includes just a simple linear relationship between them and an additional underestimation at noon may be as high as 10–12 ppb.

Validation of the AERI v2 CO retrieval algorithm was performed using independent simultaneous CO in-situ sampling from a 60-m-tall tower and aircraft sampling up to 4 km above the surface. Above 5 km, AIRS v5 retrievals were used to complete the composite ground-truth profiles. The squared correlation coefficient between ground truth CO profiles convolved with AERI averaging kernels (AK) and AERI CO retrievals is 0.57 with a slope of 0.92. However, a negative 16-ppb bias remains. At this point, we interpret this bias as an indication that the AERI retrievals are more sensitive to lower CO concentrations in the mean free troposphere (MFT) accounted for by the computed AK. A new AERI CO retrieval algorithm is in development to separately retrieve BL and MFT CO concentrations.

A comparison of simultaneously measured in situ CO in the BL and remotely in the lower 2 km supplies very useful information about changes in CO vertical distribution with high temporal resolution. For instance, during night time, the CO mixing ratio in the BL usually increases during the development of a thin, stable nocturnal BL. Conversely, CO measured by AERI does not show this effect. Near dawn the nocturnal BL is destroyed and CO is redistributed vertically. This causes a significant CO decrease near the surface, but the vertically averaged AERI CO retrievals do not change.

Comparison of the seasonal cycles of CO in the BL and that measured by AERI also is illustrative. The seasonal spring maximum of the BL CO is significantly larger than that measured by AERI due to steep CO profiles formed by the end of winter time. However, throughout May both curves converge and in June the atmosphere becomes almost well mixed. The same effect was first observed in spring-summer of 1995 in Alaska in the course of a similar experiment (Yurganov et al., 1998). Through the summer time the relation between these two data sets depends on the intensity of surface emissions, the rate of vertical mixing, and advection of CO from remote sources such as forest fires.

Deseasonalized monthly AERI CO retrievals are in agreement with satellite, surface, and total column measurements throughout the 2000s. The greatest influence on these variations was due to Siberian forest fires in 2002 and 2003, up to a 25% increase. Interestingly, this value lies between the 15% increase determined from total columns measured by AIRS (20% increase measured by MOPITT (Yurganov et al., 2005, 2009)) and the 35% increase determined from NH mid-latitude surface measurements (Yurganov et al., 2005). This confirms the intermediate altitude coverage of a sky-viewing instrument like AERI in comparison to ground-based in situ measurements and total columns measured from ground and space. Therefore, AERI measurements complement existing monitoring facilities and do not duplicate them.

Finally, after August 2008, deseasonalized CO mixing ratios measured by AERI decreased to a minimum in January 2009 before recovering. The same behavior of CO burden for North American and the entire NH mid-latitudes was observed from space by MOPITT and AIRS. The most likely explanation for this effect is a diminution of the NH CO emission from fossil fuels connected with the global economic recession. Some effect of diminished biomass burning in the tropics is possible, but a quantitative estimate of this effect requires detailed modeling of global transport.

Acknowledgements. This research was supported through a subcontract with the AIRS Project Office at JPL; by NASA grants NAG5-11653, NNG04GN42G, and NNG06GB06G; and by NOAA grant NA04AOAR4310095. The in situ measurements at the tower and the aircraft sampling were supported by the Director, Office of Science, Office of Biological and Environmental Research, Climate Change Research Division, of the US Department of Energy under Contract No. DE-AC02-05CH11231. The authors are grateful to Paul Novelli and Colm Sweeny for supplying the aircraft CO measurements and helpful comments that improved the manuscript. We thank Bruce Doddridge for his support of initial AERI CO validation during CAMEX-2.

References

ACRF: Annual Report 2008, DOE/SC-ARM-0805, http://www.arm.gov/publications/programdocs/doe-sc-arm-0805.pdf, 2008.

Backus, G. E. and Gilbert, J. F.: Uniqueness in the inversion of gross earth data, Phil. Trans. R. Soc., 266, 123–192, 1970.

Bergamaschi, P., Hein, R., Heimann, M., Crutzen, P. J.: Inverse modeling of the global CO cycle, 1, Inversion of CO mixing ratios , J. Geophys. Res., 105(D2), p. 1909 (1999JD900818), 2000.

Biraud, S. C., Torn, M., Riley, W. J., et al.: Regional Carbon Fluxes and Atmospheric Carbon Dynamics in the Southern Great Plains during the 2007 CLASIC intensive, Eos Trans. AGU, 88(52), Fall Meet. Suppl., Abstract B43D-1595, 2007.

Buchwitz, M., de Beek, R., Bramstedt, K., Noël, S., Bovensmann, H., and Burrows, J. P.: Global carbon monoxide as retrieved from SCIAMACHY by WFM-DOAS, Atmos. Chem. Phys., 4, 1945–1960, 2004, http://www.atmos-chem-phys.net/4/1945/2004/.

Candy, J.: Signal processing, the modern approach, McGraw-Hill, New-York, 1988.

Clerbaux, C., Edwards, D. P., Deeter, M., Emmons, L., Lamarque, J.-F., Tie, X. X., Massie, S. T., and Gille, J.: Carbon monoxide pollution from cities and urban areas observed by the Terra/MOPITT mission, Geophys. Res. Lett., 35, L03817, doi:10.1029/2007GL032300, 2008.

Collard, A. D., Ackerman, S. A., Smith, W. L., Ma, H. E., Revercomb, H. E., Knuteson, R. O., and Lee, C.: Cirrus cloud properties derived from High Spectral Resolution Infrared Spectrometry using FIRE II. Part III: Ground-based HIS results, J. Atmos. Sci., 52(23), 4264–4275, 1995.

Conrath, B. J.: Vertical resolution of temperature profiles obtained from remote sensing measurements, J. Atmos. Sci., 29, 1262–1271, 1972.

DeSlover, D. H., Smith, W. L., Piironen, P. K., and Eloranta, E. W.: A methodology for measuring cirrus cloud visible-to-infrared spectral optical depth ratios, J. Atmos. Ocean. Tech., 16(2), 251–262, 1999.

DeSouza-Machado, S., Strow, L., and Hannon, S.: kCompressed atmospheric radiative transfer algorithm (kCARTA), in: Satellite Remote Sensing of Clouds and the Atmosphere, Proc. of the European Symposium on Aerospace Remote Sensing #3220, Europto Series, Institute of Electrical Engineers, London, Great Britain, 1997.

Dianov-Klokov, V. I. and Yurganov, L. N.: A spectroscopic study of the global space-time distribution of atmospheric CO, Tellus, 33, 262–273, 1981.
Edwards, D. P., Emmons, L. K., Gille, J. C., Chu, A., Atti'e, J.-L., Giglio, L., Wood, S. W., Haywood, J., Deeter, M. N., Massie, S. T., Ziskin, D. C., and Drummond J. R.: Satellite-observed pollution from Southern Hemisphere biomass burning, J. Geophys. Res., 111, D14312, doi:10.1029/2005JD006655, 2006.
Fante, R. L.: Signal analysis and estimation: an introduction, John Wiley, Ney-York, 1988.
Feltz, W. F., Smith, W. L., Knuteson, R. O., Revercomb, H. E., Woolf, H. M., and Howell, H. B.: Meteorological applications of temperature and water vapor retrievals from the ground-based Atmospheric Emitted Radiance Interferometer (AERI), J. Appl. Meteor., 37(9), 857–875, 1998.
Feltz, W. F., Howell, H. B., Knuteson, R. O., Woolf, H. M., and Revercomb, H. E.: Near continuous profiling of temperature, moisture, and atmospheric stability using the atmospheric emitted radiancen interferometer (AERI), J. Appl. Meteor., 42, 584–598, 2003.
Fisher, J. A., Jacob, D. J., Purdy, M. T., Kopacz, M., Le Sager, P., Carouge, C., Holmes, C. D., Yantosca, R. M., Batchelor, R. L., Strong, K., Diskin, G. S., Fuelberg, H. E., Holloway, J. S., Hyer, E. J., McMillan, W. W., Warner, J., Streets, D. G., Zhang, Q., Wang, Y., and Wu, S.: Source attribution and interannual variability of Arctic pollution in spring constrained by aircraft (ARCTAS, ARCPAC) and satellite (AIRS) observations of carbon monoxide, Atmos. Chem. Phys., 10, 977–996, 2010, http://www.atmos-chem-phys.net/10/977/2010/.
Garcia, R. K., Howell, H. B., Knuteson, R. O., Revercomb, H. E., Best, F. A. Ciganovich, N. C., Dedecker, R. G., Dirkx, T. P., Ellington, S. C., Feltz, W. F.: Atmospheric Emitted Radiance Interferometer. Part II: Instrument Performance, J. Atmos. Oceanic Technol., 21(12), 1777–1789, 2004.
Goode, J., Yokelson, R., Susott, R., and Ward, D.: Trace gas emissions from laboratory biomass fires measured by open-path Fourier transform infrared spectroscopy: Fires in grass and surface fuels, J. Geophys. Res., 104(D17), 21237–21245, 1999.
He, H., McMillan, W. W., Knuteson, R. O., Feltz, W. F.: Tropospheric carbon monoxide column density retrieval during Pre-launch MOPITT Validation exercise, Atmos. Environ., 35(3), 509–514, doi:10.1016/S1352-2310(00)00334-4, 2001.
Knuteson, R. O, Revercomb, H. E., Best, F. A., Ciganovich, N. C, Dedecker, R. G., Dirkx, T. P., Ellington, S. C., Feltz, W. F., Garcia, R. K., and Howell, H. B.: Atmospheric Emitted Radiance

Interferometer. Part I: Instrument Design, J. Atmos. Ocean. Technol., 21(12), 1763–1776, 2004.

Kopacz, M., Jacob, D. J., Fisher, J. A., Logan, J. A., Zhang, L., Megretskaia, I. A., Yantosca, R. M., Singh, K., Henze, D. K., Burrows, J. P., Buchwitz, M., Khlystova, I., McMillan, W. W., Gille, J. C., Edwards, D. P., Eldering, A., Thouret, V., and Nedelec, P.: Global estimates of CO sources with high resolution by adjoint inversion of multiple satellite datasets (MOPITT, AIRS, SCIAMACHY, TES), Atmos. Chem. Phys., 10, 855–876, 2010, http://www.atmos-chem-phys.net/10/855/2010/.

Liljegren, J. C.: Two-channel microwave radiometer for observations of total column precipitable water vapor and cloud liquid water path, Fifth Symposium on Global Change Studies, 23–28 January 1994, American Meteorological Society, Nashville, Tennessee, 262–269, 1994.

McMillan, W. W., Strow, L. L., Smith, W. L., Revercomb, H. E., and Huang, H. L.: The detection of enhanced carbon monoxide abundances in remotely sensed infrared spectra of a forest fire smoke plume, Geophys. Res. Lett., 23(22), 3199–3202, 1996.

McMillan, W. W., Strow, L. L., Smith, W. L., Revercomb, H. E., Huang, H. L., Ryan, W. F., Thompson, A. M., and McNamara, D. P.: Remote sensing of CO over the continental US on September 12-13, 1993, J. Geophys. Res., 102(D9), 10695–10709, 1997.

McMillan, W. W., He, H., Doddridge, B. G., Feltz, W. F., Knuteson, R. O., McKernan, E., Pougatchev, N. S., Smith, W. L., Strow, L. L., Wang, J., and Yurganov, L.: Validation of carbon monoxide retrievals from up-looking FTIR atmospheric thermal emission spectra, in: Optical Remote Sensing of the Atmosphere, Optical Society of America Technical Digest, 163–165, 1999.

McMillan, W. W., McCourt, M., Revercomb, H., Knuteson, R. O., Christian, T. J., Doddridge, B. G., Hobbs, P. V., Lukovich, J. V., Novelli, P. C., Piketh, S. J., Sparling, L., Stein, D., Swap, R. J., and Yokelson, R. J.: Tropospheric carbon monoxide measurements from the Scanning High-resolution Interferometer Sounder on September 7, 2000, in southern Africa during SAFARI, J. Geophys. Res., 108(D13), 8492, doi:10.1029/2002JD002335, 2003.

McMillan, W. W., Barnet, C., Strow, L., Chahine, M. T., McCourt, M. L., Warner, J. X., Novelli, P. C., Korontzi, S., Maddy, E. S., and Datta, S.: Daily global maps of carbon monoxide from NASA's Atmospheric Infrared Sounder, Geophys. Res. Lett., 32, L11801, doi:10.1029/2004GL021821, 2005.

McMillan, W. W. and Yurganov, L.: Local, regional, and global views of tropospheric carbon monoxide from the Atmospheric Infrared Sounder (AIRS), Proceedings of SPIE, 6966, Al-

gorithms and Technologies for Multispectral, Hyperspectral, and Ultraspectral Imagery XIV, edited by: Shen, S. S. and Lewis, P. E., 696615 (11 Apr 2008), doi:10.1117/12.776983, 2008a.

McMillan, W. W., Warner, J. X., McCourt Comer, M., Maddy, E., Chu, A., Sparling, L., Eloranta, E., Hoff, R., Sachse, G., Barnet, C., Razenkov, I., and Wolf, W.: AIRS views transport from 12 to 22 July 2004 Alaskan/Canadian fires: Correlation of AIRS CO and MODIS AOD with forward trajectories and comparison of AIRS CO retrievals with DC-8 in situ measurements during INTEX-A/ICARTT, J. Geophys. Res., 113, D20301, doi:10.102009/2007JD009711, 2008b.

McMillan, W. W., Evans, K. Barnet, C., Maddy, E., Sachse, G., and Diskin, G.: AIRS Version 5 CO Retrieval: Algorithm Description and Validation, IEEE Trans. Geosci. Remote Sens., submitted, November 2009.

McMillan, W. W., Pierce, R., Sparling, L. C., Osterman, G., McCann, K., Fischer, M. L., Rappenglueck, B., Newton, R., Turner, D. D., Kittaka, C., Evans, K., Biraud, S., Lefer, B., Andrews, A., and Oltmans, S.: An Observational and modeling strategy to investigate the impact of remote sources on local air quality: A Houston, Texas case study from TEXAQS II, J. Geophys. Res., 115, D01301, doi:10.1029/2009JD011973, 2010.

Minnett, P. J., Knuteson, R. O., Best, F. A., Osborne, B. J., Hanafin, J. A., and Brown, O. B.: The Marine-Atmospheric Emitted Radiance Interferometer: A High-Accuracy, Seagoing Infrared Spectroradiometer, J. Atmos. Ocean. Technol., 18, 994–1013, 2001.

Nalli, N. R., Minnett, P. J., and van Delst, P.: Emissivity and reflection model for calculating unpolarized isotropic water surface-leaving radiance in the infrared. I: Theoretical development and calculations, Appl. Optics, 47(21), 3701–3721, 2008.

Nedelec, P., Cammas, J.-P., Thouret, V., Athier, G., Cousin, J.-M., Legrand, C., Abonnel, C., Lecoeur, F., Cayez, G., and Marizy, C.: An improved infrared carbon monoxide analyser for routine measurements aboard commercial Airbus aircraft: technical validation and first scientific results of the MOZAIC III programme, Atmos. Chem. Phys., 3, 1551–1564, 2003, http://www.atmos-chem-phys.net/3/1551/2003/.

Novelli, P. C., Elkins, J. W., and Steele, L. P.: The development and evaluation of a gravimetric reference scale for measurements of atmospheric carbon monoxide, J. Geophys. Res., 96, 13109–13121, 1991.

Novelli, P. C., Connors, V. S., Reichle Jr., H. G., et al.: An internally consistent set of globally distributed atmospheric carbon monoxide mixing ratios developed using results from an

intercomparison of measurements, J. Geophys. Res., 103(D15), 19285–19293, 1998.
Novelli, P. C., Masarie, K. A., Lang, P. M., Hall, B. D., Myers, R. C., and Elkins, J. W.: Reanalysis of tropospheric CO trends: Effects of the 1997–1998 wildfires, J. Geophys. Res., 108(D15), 4464, doi:10.1029/2002JD003031, 2003.
Potosnak, M. J., Wofsy, S. C., Denning, A. S., Conway, T. J., Munger, J. W., and Barnes, D. H.: Influence of biotic exchange and combustion sources on atmospheric CO2 concentrations in New England from observations at a forest flux tower, J. Geophys. Res., 104, 9561–9569. 1999.
Reichle, H., Connors, V., Holland, J., Sherrill, R., Wallio, H., Casas, J., Condon, E., Gormsen, B., and Seiler, W.The distribution of middle tropospheric CO during early October 1984, J. Geophys. Res., 95, 9845–9856, 1990.
Rinsland, C. P., Jones, N. B., Connor, B. J., Logan, J. A., Pougatchev, N. S., Goldman, A., Murcray, F. J., Stephen,T. M., Pine, A. S., Zander, R., Mahieu, E., and Demoulin, P.: Northern and southern hemisphere ground-based infraredspectroscopic measurements of tropospheric carbon monoxideand ethane, J. Geophys. Res., 103(D21), 28197–28218, doi:10.1029/98JD02515, 1998.
Rinsland, C. P., Paton-Walsh, C., Jones, N. B., Griffith, D. W. T., Goldman, A., Wood, S. W., Chiou, L., and Meier, A.: High spectral resolution solar absorption measurements of ethylene (C_2H_4) in a forest fire smoke plume using HITRAN parameters: Tropospheric vertical profile retrieval, J. Quant. Spectrosc. Rad. Transfer, 96, 301–309, 2005.
Rodgers, C. D. and Connor, B. J.: Intercomparison of remote sounding instruments, J. Geophys. Res., 108(D3), 4116, doi:10.1029/2002JD002299, 2003.
Rothman, L. S., Jacquemart, D., Barbe, A., Benner, D. C., Birk, M., Brown, L. R., Carleer, M. R., Chackerian, C., Chance, K., Coudert, L. H., Dana, V., Devi, V. M., Flaud, J. M., Gamache, R. R., Goldman, A., Hartmann, J. M., Jucks, K. W., Maki, A. G., Mandin, J. Y., Massie, S. T., Orphal, J., Perrin, A., Rinsland, C. P., Smith, M. A. H., Tennyson, J., Tolchenov, R. N., Toth, R. A., Vander Auwera, J., Varanasi, P., and Wagner, G.: The HITRAN 2004 molecular spectroscopic database, J. Quant. Spectrosc. Rad. Transfer, 96, 139–204, 2005.
Smith, W. L., Feltz, W. F., , Knuteson, R. O., Revercomb, H. B., Howell, H. B., and Woolf, H. M.: The retrieval of planetary boundary layer structure using ground-based infrared spectral radiance measurements, J. Atmos. Ocean. Technol., 16, 323–333, 1999.
Sachse, G. W., Hill, G. F., Wade, L. O., and Perry, M. G.: Fast-response, high-precision carbon monoxide sensor using a tunable diode laser absorption technique, J. Geophys. Res., 92,

2071–2081, 1987.
Spivakovsky, C. M., Logan, J. A., Montzka, S. A., et al.: Three-dimensional climatological distribution of tropospheric OH: Update and evaluation, J. Geophys. Res., 105, 8931–8980, 2000.
Turner, D. D., Feltz, W. F., and Ferrare, R. A.: Continuous water vapor profiles from operational ground-based active and passive remote sensors, B. Am. Meteorol. Soc., 81, 1301–1317, 2000.
Turner, D. D., Tobin, D. C., Clough, S. A., Brown, P. D., Ellingson, R. G., Mlawer, E. J., Knuteson, R. O., Revercomb, H. E., Shippert, T. R., Smith, W. L., and Shephard, M. W.: The QME AERI LBLRTM: A Closure Experiment for Downwelling High Spectral Resolution Infrared Radiance, J. Atmos. Sci., 61, 2657–2675, 2004.
Turner, D. D., Clough, S. A., Liljegren, J. C., Clothiaux, E. E., Cady-Pereira, K., and Gaustad, K. L.: Retrieving precipitable water vapor and liquid water path from Atmospheric Radiation Measurement (ARM) program's microwave radiometers, IEEE Trans. Geosci. Remote Sens., 45(11), 233–252, 2007.
Turquety, S., Hurtmans, D., Hadji-Lazaro, J., Coheur, P.-F., Clerbaux, C., Josset, D., and Tsamalis, C.: Tracking the emission and transport of pollution from wildfires using the IASI CO retrievals: analysis of the summer 2007 Greek fires, Atmos. Chem. Phys., 9, 4897–4913, 2009, http://www.atmos-chem-phys.net/9/4897/2009/.
Wang, J., Gille, J. C., Bailey, P. L., Shertz, S., Smith, M., Drummond, J. R., McKernan, E., Tolton, B., Yurganov, L., Jones, N. B., Gore, B., Novelli, P., He, H., McMillan, W. W., Murcray, F., Stephen, T., Pougatchev, N., and Reichle, H. G.: The Pre-launch MOPITT Validation Exercise (Pre-MOVE), The Earth Observer 11, 5–9, 1999.
Yurganov, L. N., Jaffe, D. A., Pullman, E., and Novelli, P. C.: Total column and surface densities of atmospheric carbon monoxide in Alaska, 1995, J. Geophys. Res., 103, 19337–19346, 1998.
Yurganov, L. N., Duchatelet, P., Dzhola, A. V., Edwards, D. P., Hase, F., Kramer, I., Mahieu, E., Mellqvist, J., Notholt, J., Novelli, P. C., Rockmann, A., Scheel, H. E., Schneider, M., Schulz, A., Strandberg, A., Sussmann, R., Tanimoto, H., Velazco, V., Drummond, J. R., and Gille, J. C.: Increased Northern Hemispheric carbon monoxide burden in the troposphere in 2002 and 2003 detected from the ground and from space, Atmos. Chem. Phys., 5, 563–573, 2005, http://www.atmos-chem-phys.net/5/563/2005/.

AMTD
3, 1263–1301, 2010

Yurganov, L., McMillan, W., Dzhola, A., Grechko, E., Jones, N., and van der Werf, G.: Global AIRS and MOPITT CO Measurements: Validation, Comparison, and Links to Biomass Burning Variations and Carbon Cycle, J. Geophys. Res., 113, D09301, doi:10.1029/2007JD009229, 2008.

Yurganov, L. N., McMillan, W., Grechko, E., and Dzhola, A.: Analysis of global and regional CO burdens measured from space between 2000 and 2009 and validated by ground-based solar tracking spectrometers, Atmos. Chem. Phys. Discuss., 9, 24875–24911, 2009, http://www.atmos-chem-phys-discuss.net/9/24875/2009/.

Zander, R., Demoulin, P., Ehhalt, D. H., Schmidt, U., Rinsland, C. P.: Secular increase of total vertical column abundance of carbon monoxide above Central Europe since 1950, J. Geophys. Res., 94, 11021–11028, 1989.

Zhang, L., Jacob, D. J., Boersma, K. F., Jaffe, D. A., Olson, J. R., Bowman, K. W., Worden, J. R., Thompson, A. M., Avery, M. A., Cohen, R. C., Dibb, J. E., Flock, F. M., Fuelberg, H. E., Huey, L. G., McMillan, W. W., Singh, H. B., and Weinheimer, A. J.: Transpacific transport of ozone pollution and the effect of recent Asian emission increases on air quality in North America: an integrated analysis using satellite, aircraft, ozonesonde, and surface observations, Atmos. Chem. Phys., 8, 6117–6136, 2008, http://www.atmos-chem-phys.net/8/6117/2008/.

AMTD

3, 1263–1301, 2010

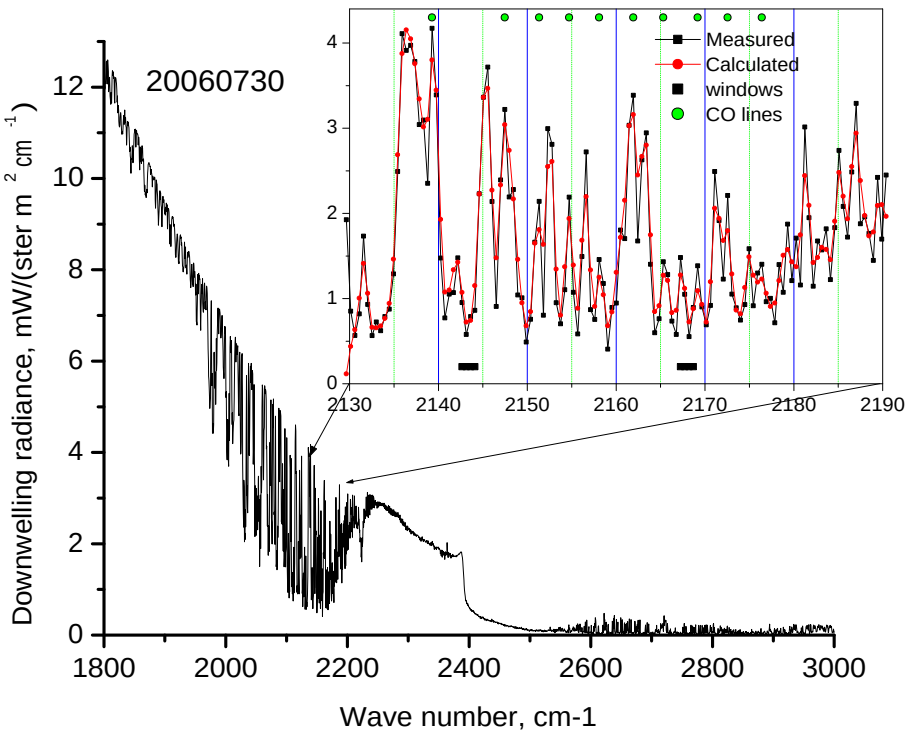

Fig. 1. An example spectrum of atmospheric zenith sky radiances measured by the SGP AERI on 30 July 2006 at 12:45 UTC together with that calculated for the constant CO profile with mixing ratio 78.4 ppb (inserted). Green circles indicate locations of CO lines. Black bars correspond to locations of transparent windows used for estimates of scattered solar radiance.

AMTD
3, 1263–1301, 2010

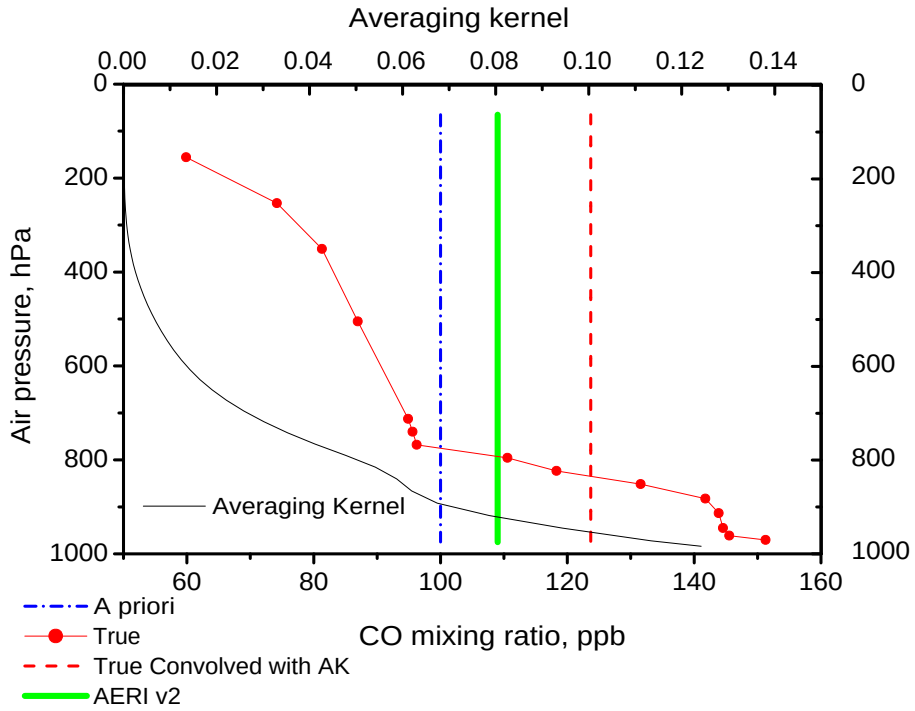

Fig. 2. AERIv2 is the mean CO mixing ratio retrieved from AERI spectrum for 17:00–18:00 UTC, 28 September 2008. Also plotted are the 100 ppbv a priori CO profile, the CO averaging kernel calculated for the given conditions, the true CO profile, and a profile derived by convolution of the previous three. The true profile is built from the in-situ tower measurement (the lowermost symbol corresponding to 60 m above the surface), in situ aircraft data (below 600 hPa level and between 16:36 and 18:15 UTC), and the four uppermost points are from AIRS v5 L3 product for that day around 19:30 UTC.

AMTD
3, 1263–1301, 2010

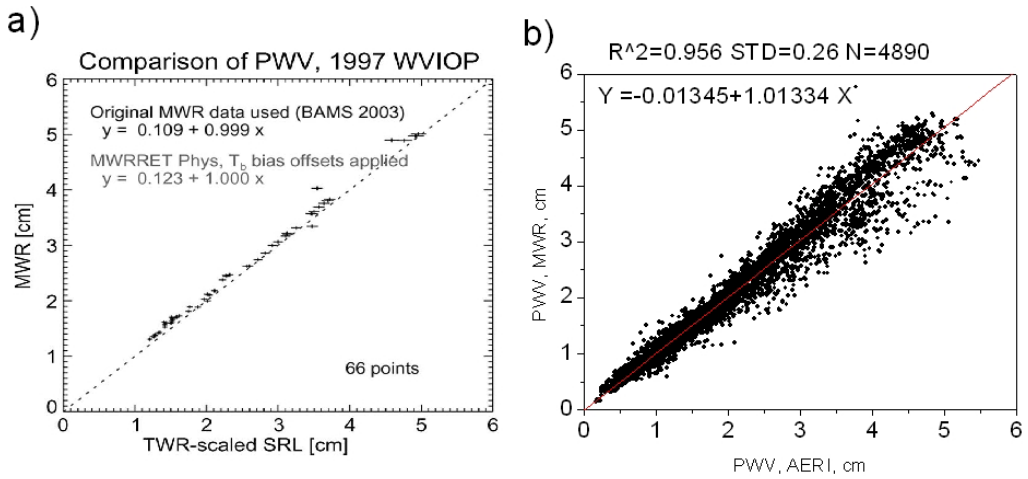

Fig. 3. **(a)** Adopted from Turner et al. (2007), comparison of PWV derived from the scanning Raman lidar (x-axis) and the MWR retrievals (y-axis) during clear-sky periods of the 1997 WVIOP. The squared correlation coefficient is 0.994. **(b)** Comparison of PWV retrieved from AERI spectra and from MWR data during 2006. The squared correlation coefficient is 0.956.

AMTD
3, 1263–1301, 2010

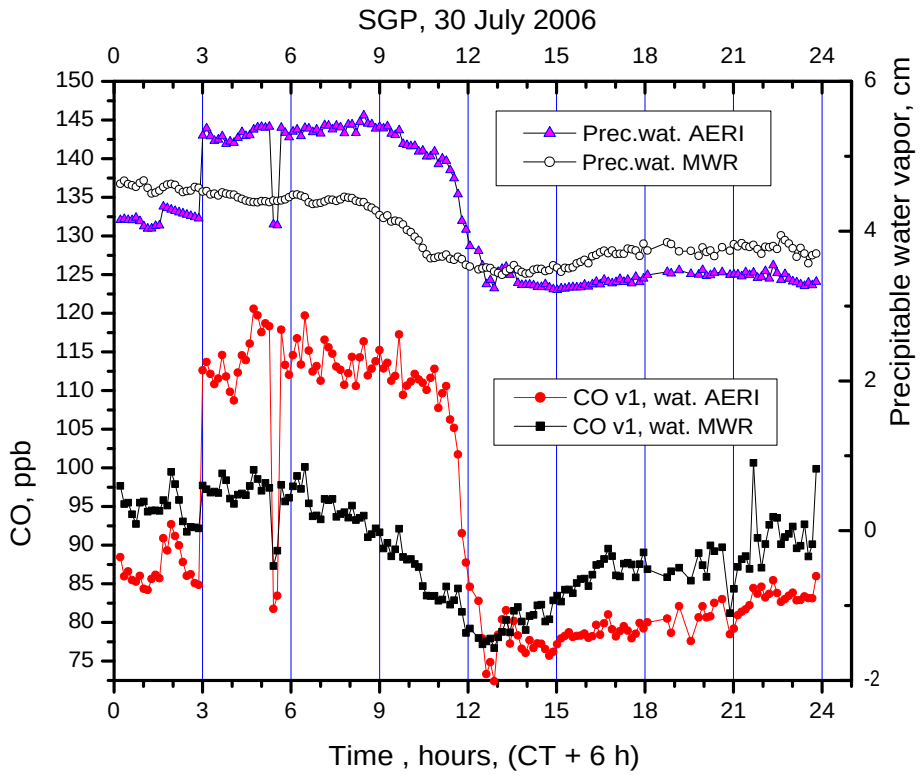

Fig. 4. An example AERI-derived PWV compared with MWR-derived PWV (top two curves). Bottom two curves are CO retrievals with input water vapor profiles from AERI spectra (red) and AERI-derived water vapor profile scaled using MWR PWV (black).

AMTD
3, 1263–1301, 2010

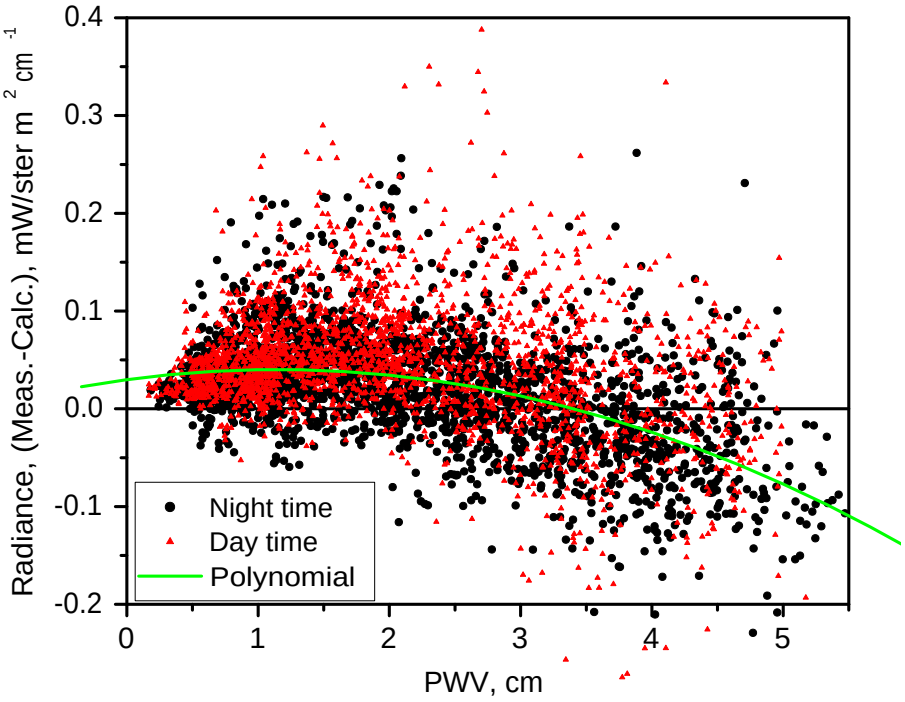

Fig. 5. Radiances averaged over 2 spectral intervals taken together: between 2142.7–2144.1 cm^{-1} and 2167.2–2168.7 cm^{-1} used for verification of kCARTA calculations. Differences between measured and calculated radiances for day time and night time are plotted as a function of PWV.

AMTD
3, 1263–1301, 2010

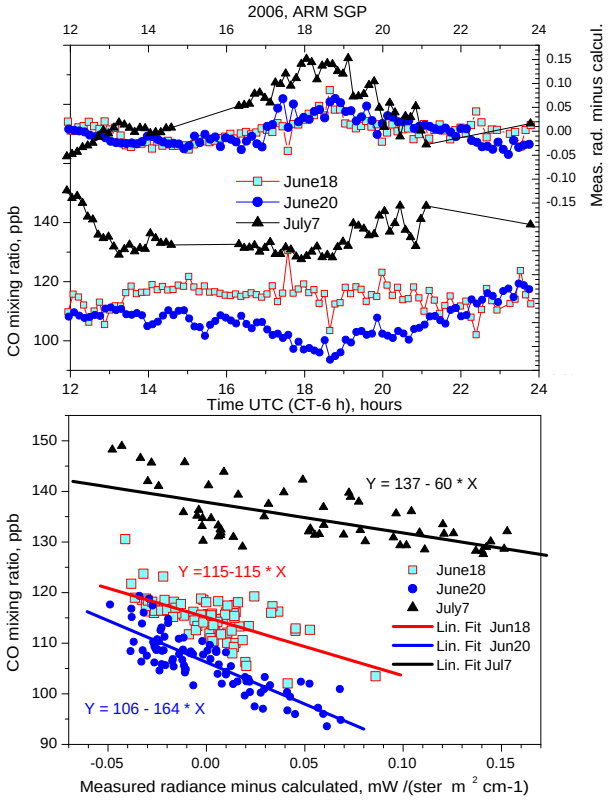

Fig. 6. Top panel: The top three curves (right y-axis) illustrate the radiance differences (RD) for three days in 2006 between measured AERI and computed radiances in two transparent windows in the CO band (see Fig. 1). The bottom three curves (left y-axis) show the corresponding CO retrieved from the AERI spectra for these days. Bottom panel: The CO and RD points from the top panel are plotted against each other for each of the three days along with best fit regression lines.

AMTD
3, 1263–1301, 2010

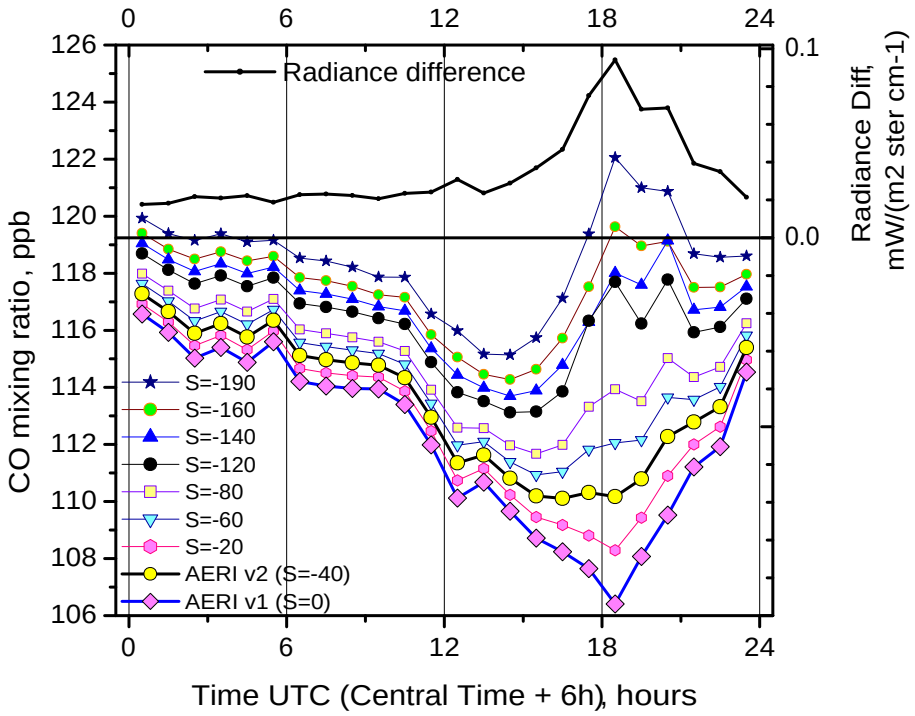

Fig. 7. Top curve and right scale: a difference between measured and calculated radiance (RD) in the windows. Bottom curves and left scale: mean diurnal cycles of CO mixing ratio retrieved from AERI spectra for 2006 and corrected for the scattered light using for different slopes, S, of the correlation between CO and RD. The AERI v2 curve corresponds to the slope of −40 where the anticorrelation of CO and RD minimizes.

AMTD
3, 1263–1301, 2010

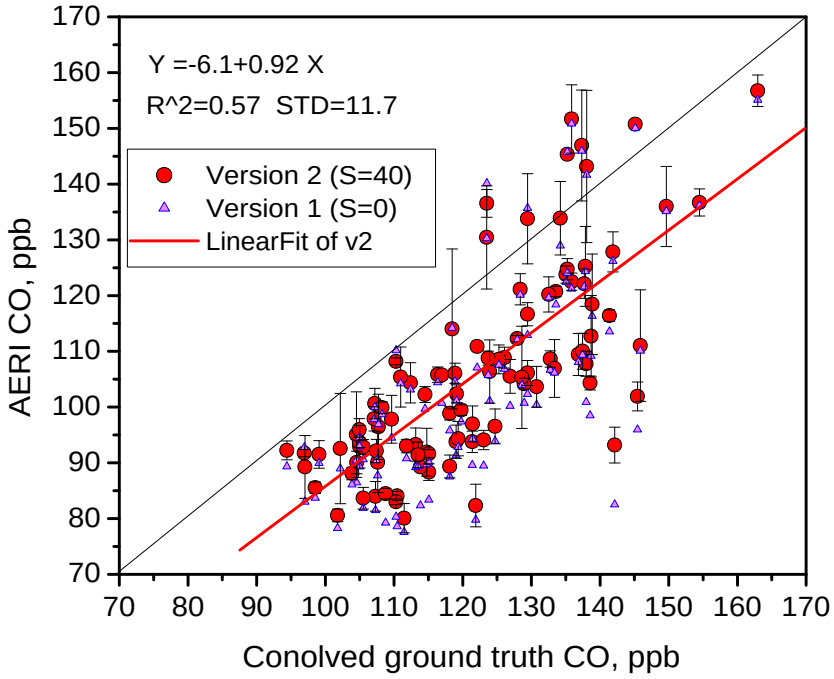

Fig. 8. Comparison of v1 and v2 CO mixing ratios retrieved from AERI spectra with convolved composite ground-truth profiles (see Fig. 2).

AMTD
3, 1263–1301, 2010

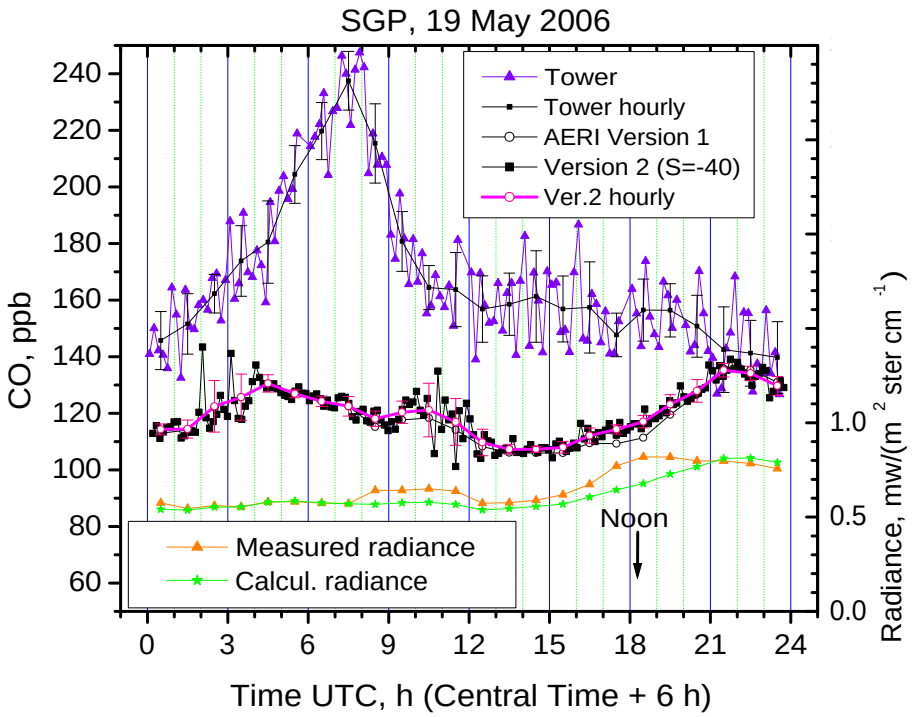

Fig. 9. Example measurement results for clear sky conditions of 19 May 2006. The differences between the two versions of AERI retrievals are proportional to the radiance differences (bottom two curves) and amount to ~5 ppbv around noon for this specific day.

AMTD
3, 1263–1301, 2010

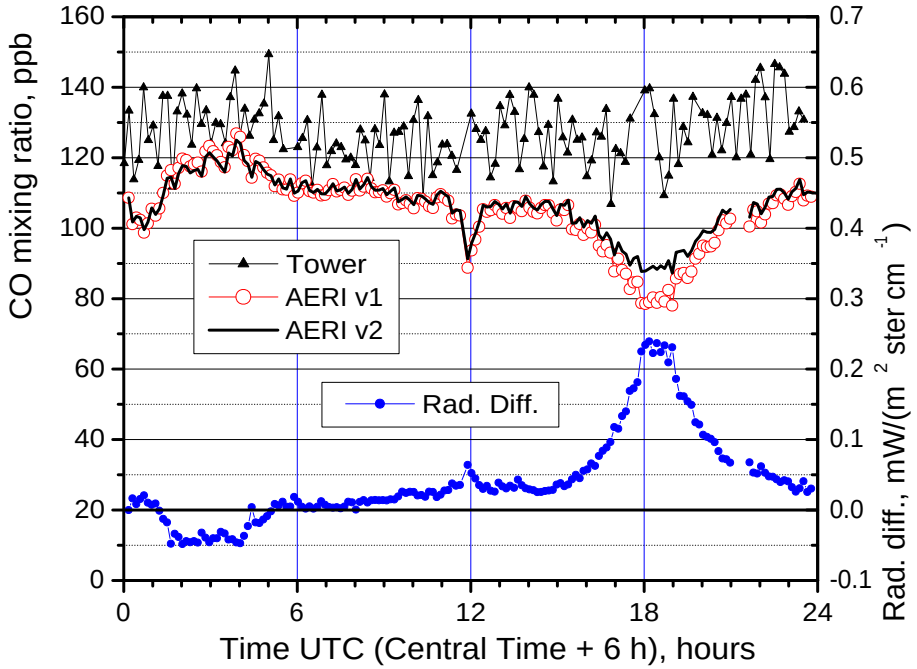

Fig. 10. Example measurement results for clear sky conditions of 8 June 2007. A difference between measured and calculated window radiances RD (blue dots) anticorrelates with AERI CO v1 around local noon (slope = −198, $R^2 = 0.92$). Although the amplitude around noon for AERI CO v2 is less, it appears the correction for scattered sunlight is not complete.

AMTD
3, 1263–1301, 2010

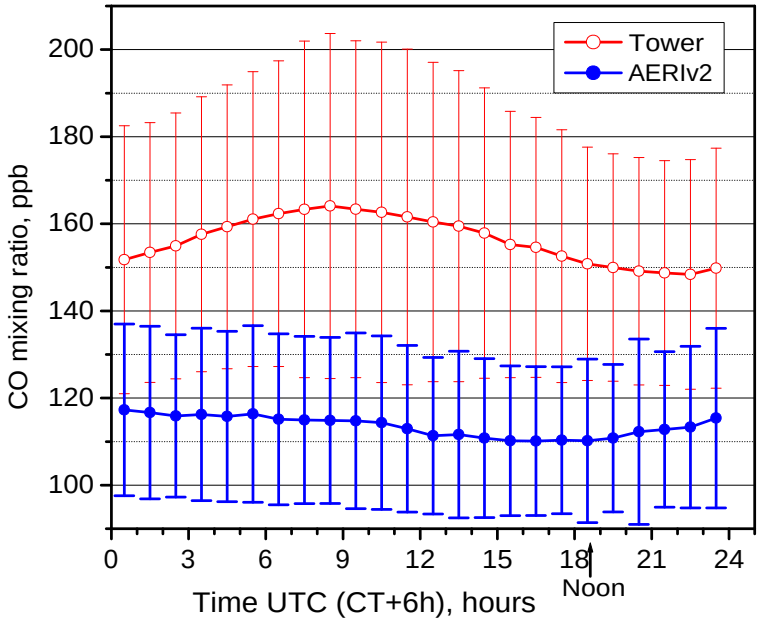

Fig. 11. Average 2006 diurnal cycles for in-situ measurements at the 60-m-tall tower and CO retrieved from AERI v2. Vertical bars are the standard deviations of hourly means.

AMTD
3, 1263–1301, 2010

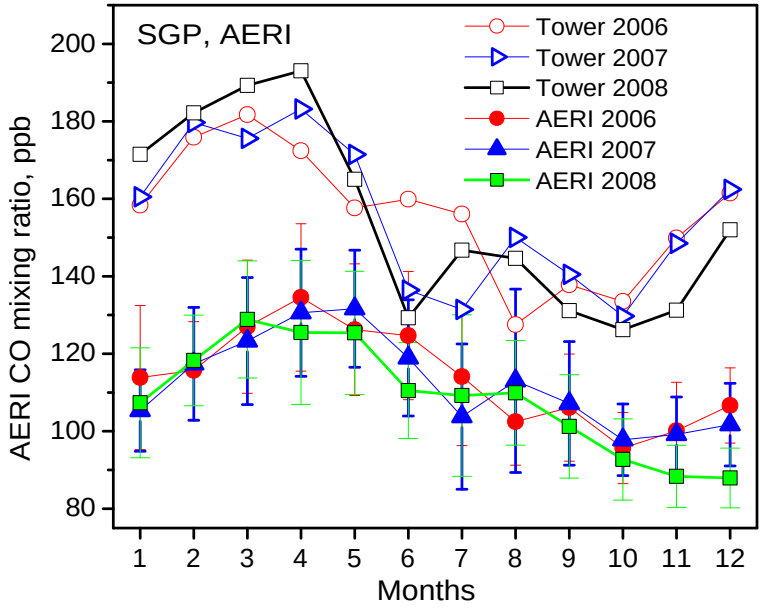

Fig. 12. Mean seasonal cycles for 3 years of simultaneous in-situ and remote sensing CO observations at the SGP.

AMTD
3, 1263–1301, 2010

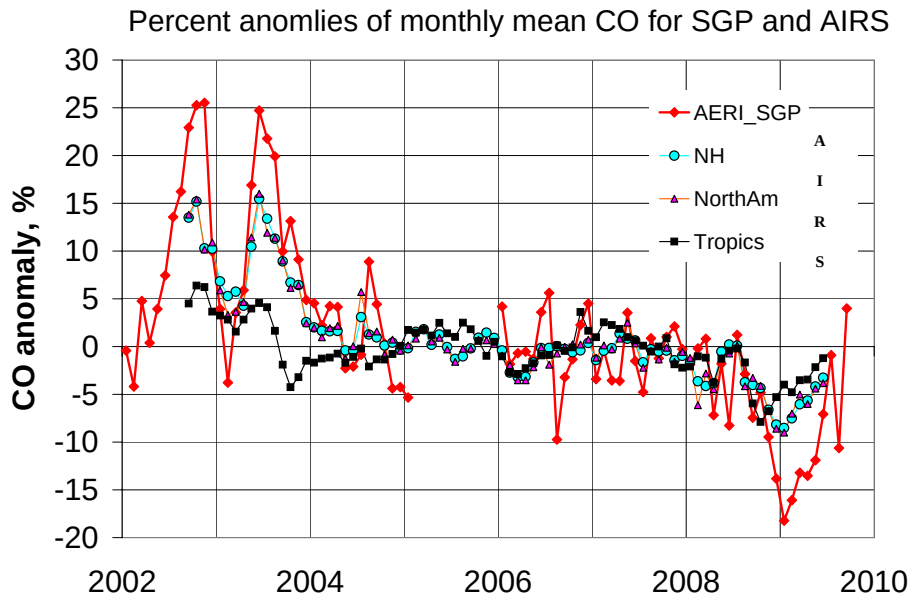

Fig. 13. Anomalies of monthly mean CO retrieved by AERI v2 referenced to the seasonal cycle calculated from the period from January 2004 through December 2007. Plotted for comparison are total column CO anomalies for the NH (between 30 N and 70 N), North America (bounded by 30 N, 70 N; 60 W, 170 W), and the tropical belt (30 S–30 N) measured by AIRS and corrected according to Yurganov et al. (2009.

AMTD
3, 1263–1301, 2010